JACS
JOURNAL OF THE AMERICAN CHEMICAL SOCIETY
pubs.acs.org/JACS
Article

Dissolution of the Solid Electrolyte Interphase and Its Effects on Lithium Metal Anode Cyclability

Philaphon Sayavong, Wenbo Zhang, Solomon T. Oyakhire, David T. Boyle, Yuelang Chen, Sang Cheol Kim, Rafael A. Vilá, Sarah E. Holmes, Mun Sek Kim, Stacey F. Bent, Zhenan Bao, and Yi Cui*

Cite This: https://doi.org/10.1021/jacs.3c03195

ABSTRACT: At >95% Coulombic efficiencies, most of the capacity loss for Li metal anodes (LMAs) is through the formation and growth of the solid electrolyte interphase (SEI). However, the mechanism through which this happens remains unclear. One property of the SEI that directly affects its formation and growth is the SEI's solubility in the electrolyte. Here, we systematically quantify and compare the solubility of SEIs derived from ether-based electrolytes optimized for LMAs using *in-operando* electrochemical quartz crystal microbalance (EQCM). A correlation among solubility, passivity, and cyclability established in this work reveals that SEI dissolution is a major contributor to the differences in passivity and electrochemical performance among battery electrolytes. Together with our EQCM, X-ray photoelectron spectroscopy (XPS), and nuclear magnetic resonance (NMR) spectroscopy results, we show that solubility depends on not only the SEI's composition but also the properties of the electrolyte. This provides a crucial piece of information that could help minimize capacity loss due to SEI formation and growth during battery cycling and aging.

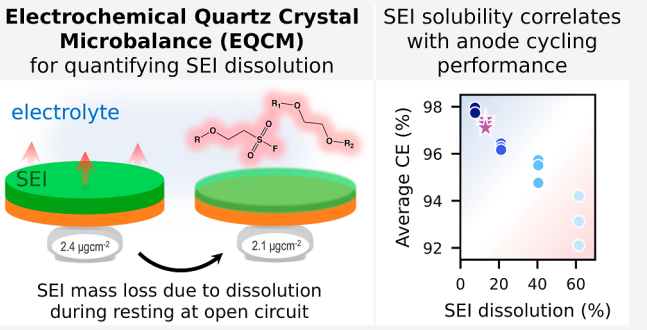

INTRODUCTION

Despite their potential to provide higher energy density rechargeable batteries, lithium metal anodes (LMA) suffer from low cyclability. The two major capacity fading mechanisms that result in low cycle life include (1) the isolation of electroactive lithium (Li) metal deposits from the current collector and (2) continuous reduction of the electrolyte with electroactive surfaces in the anode to form the solid electrolyte interphase (SEI).[1−3] The passivating SEI layer mitigates the thermodynamic instability of Li metal toward the electrolyte, preventing further reactions that result in lower Coulombic efficiency (CE, ratio of capacity output during discharge to capacity input during charge). Recent advancements in liquid electrolyte engineering have enabled highly reversible LMAs with CEs well above 95%. At such high CE, most of the capacity loss is due to SEI formation and growth.[4] However, the mechanism(s) of SEI growth remains elusive.

One property of the SEI that directly affects its formation and growth is its solubility in the electrolyte. Dissolution compromises the efficacy of the passivation layer since additional electrolyte and Li must be consumed to repair the partially dissolved SEI, resulting in a thickened layer.[5,6] Wood *et al.* predicted that SEI dissolution can completely deplete Li metal inventory before the electrolyte is consumed during cell cycling, or even after calendar aging for 80 days.[7] Furthermore, Boyle *et al.* experimentally showed an average of 2−3% CE loss after calendar aging for 24 h through the growth of the SEI on Li metal surface, even for top performing electrolytes. Their observation of organic-rich clusters after aging suggests that the growth mechanism involves the dissolution of organic components in the SEI, followed by their redeposition after locally saturating the electrolyte.[8] These previous studies indicate that SEI dissolution is a major contributor toward capacity loss through SEI formation and growth for high-performance electrolytes.

Anion-derived inorganic species within the SEI, namely, lithium fluoride (LiF), have been shown to exhibit low solubility in the electrolyte, while solvent-derived organic components can undergo significant dissolution after their formation.[7,9−12] As a result, the amount of anion-derived components in the SEI has been used to compare the solubility of SEIs derived from different electrolytes. However, Huang *et*

Received: March 29, 2023

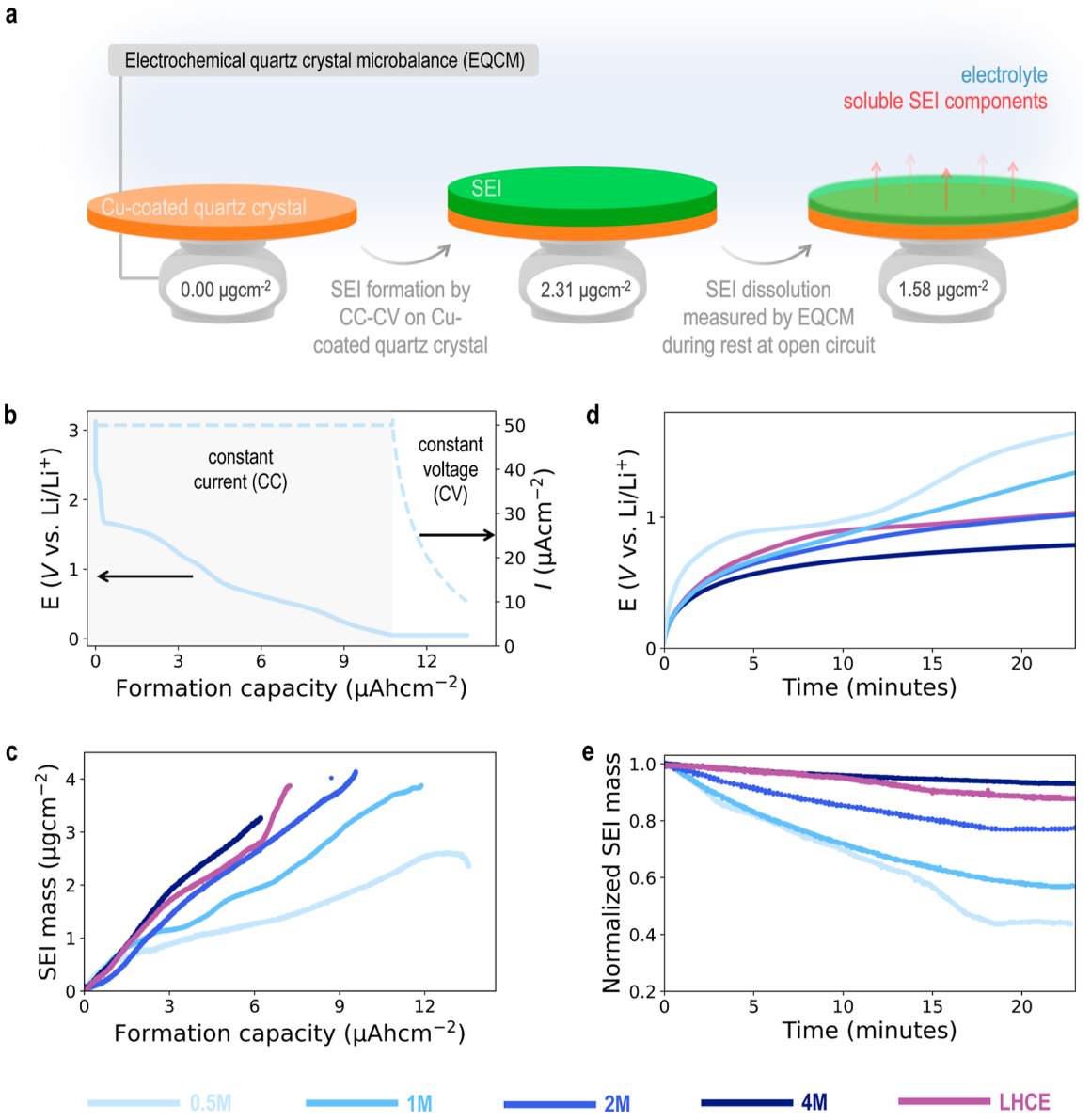

Figure 1. (a) Procedure for SEI formation and dissolution utilizing EQCM technique. (b) Potential difference and current density during SEI formation step using CC−CV protocol for 0.5 M. (c) Mass response during SEI formation. (d) Open circuit voltage during the SEI dissolution step. (e) Mass response during dissolution step, the mass presented is normalized to the final mass recorded during formation step in (d). See an all-inclusive figure that includes all the relevant measurement for 0.5 M at Figure S1. Repeats of the EQCM mass response for dissolution can be found at Figure S2.

al. recently showed evidence suggesting that LiF does not deposit directly into the compact SEI due to its moderate solubility in the electrolyte.[13] In contrast, Shadike *et al.* revealed that nanocrystalline LiF does exist within the compact SEI when a different electrolyte is used,[14] indicating that LiF solubility depends on both electrolyte chemistry and SEI composition. Their results suggest that an alternative metric that considers both the electrolyte and SEI composition is required to reliably evaluate solubility.

Recently, Kwon *et al.* utilized the electrochemical quartz crystal microbalance (EQCM)—a technique that can measure mass changes in the ng cm^{-2} scale—to quantify SEI mass loss during resting at open circuit after its formation *in situ*. They illustrated that over half of the SEI mass is loss during rest, demonstrating the potential of EQCM as a technique to accurately quantify SEI dissolution.[15] Moreover, mass loss during dissolution would be a reliable metric to compare SEI solubility, as the measurement considers solute (SEI)−solvent (electrolyte) interactions as a whole. However, this has not been widely applied to the electrolytes engineered for LMAs. Being able to quantify and compare the SEI solubility between different high-performance electrolytes could reveal the mechanism of SEI formation and growth.

Herein, we systematically quantify the dissolution of SEIs derived from the electrolytes optimized for LMAs using EQCM. Comparing SEI solubility results with performance metrics obtained from coulometric experiments allowed us to establish a correlation among solubility, passivity, and cyclability. Building upon this, we illustrate that cycle life can be further extended for one of the best electrolytes by shifting the SEI solubility equilibria, signifying that dissolution is one of the major mechanisms that induces the interphase's degrada-

https://doi.org/10.1021/jacs.3c03195
J. Am. Chem. Soc. XXXX, XXX, XXX−XXX

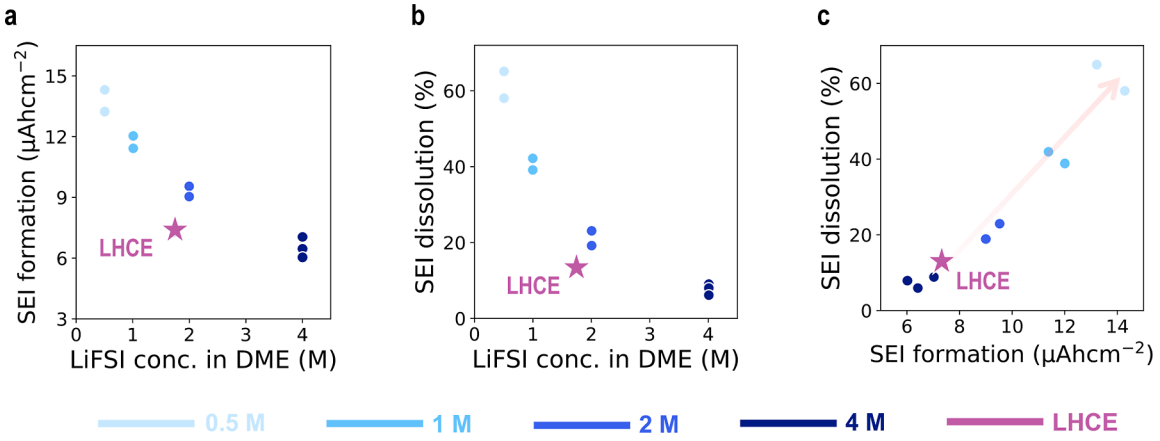

Figure 2. Relationship between (a) SEI dissolution and (b) SEI formation capacity with LiFSI concentration in the electrolytes used. (c) Relationship between SEI dissolution and SEI formation to illustrate the impact of SEI solubility on passivity.

tion and its subsequent repair. Chemical characterization of the interphase and electrolyte reveals that dissolution depends on not only the SEI's composition, but also the physical and chemical properties of the electrolyte. This is an important piece of information that introduces another design principle to minimize capacity loss during Li metal battery cycling and calendar aging.

RESULTS AND DISCUSSION

Systematic Quantification of SEI Dissolution Using EQCM. To accurately quantify the overall solubility of the SEI, EQCM is used to detect mass changes of the nanoscale interphase *in situ* (Figure 1a). EQCM has been previously used extensively to probe battery interphases.[16−19] However, few studies have focused on high-performance electrolytes tailored for LMAs. In this study, the SEI is electrochemically formed on the copper-coated quartz crystal sensor utilizing a constant current−constant-voltage (CC−CV) protocol, with a final voltage of 50 mV above lithium plating potential (Figure 1b). The potential for the CC−CV protocol allows SEI dissolution to be probed without the influence of electrodeposited lithium, while maintaining chemistry similar to SEI formed on Li metal surface.[8,20] After formation, the mass of the SEI is further monitored at open circuit to quantify the amount of soluble components in the SEI (Figure 1a). Losses in SEI mass should be due to the overall dissolution of the SEI, whether it is from the direct dissolution of the SEI, or from the dissolution of soluble species resulting from SEI decomposition. In addition, prior studies have demonstrated that SEI decomposition into gaseous product is negligible during open circuit resting at room temperatures.[21,22] Therefore, mass losses observed during our EQCM measurements should primarily be from SEI dissolution.

We systematically vary the salt concentration of the electrolytes used to form the SEI to extract physical insights from our EQCM measurements. This includes 0.5, 1, 2, and 4 M of lithium bis(fluorosulfonyl)imide (LiFSI) in 1,2-dimethoxyethane (DME), denoted as 0.5, 1, 2, and 4 M hereafter. By adding a diluent (1,1,2,2-tetrafluoroethyl 2,2,3,3-tetrafluororopyl ether, TTE) into the electrolyte, we further investigate the effect of localized high concentration environment on SEI solubility (also known as localized high concentration electrolyte, LHCE). Overall, this represents some of the commonly studied electrolytes for LMA, including some of the highest performing electrolytes (4 M and LHCE).[23,24]

During the polarization of copper-coated quartz sensors, there is a mass increase from the electroreduction of electrolytes to form SEIs (Figure 1c). The recorded SEI mass ranges from around 2 to 4 μgcm^{-2} for the electrolytes investigated, comparable with previously reported SEI mass using the same technique.[16,17] During the subsequent resting step at open circuit, the voltage profile shows a rapid voltage increase for all electrolytes investigated. However, this is not reliable evidence for SEI dissolution, as the voltage response will be different for different electrolytes (Figure 1d). Meanwhile, the mass decrease during this period shows significant SEI dissolution for all electrolytes investigated (Figure 1e). Our results show that SEI derived from 0.5 M undergoes the most dissolution, where ∼60% of its mass is loss after dissolution. In fact, the mass of the SEI decreases toward the end of its formation stage during the constant-voltage step (Figure 1c). This can be rationalized by considering the rate of mass changes from different processes. During the constant-voltage step (Figure 1b), the SEI formation rate decreases due to a decrease in current density, resulting in a slower rate of mass gain. The overall mass decline during this step indicates that mass loss from SEI dissolution occurs at a faster rate than mass gain from the formation for 0.5 M. Despite the net SEI mass loss during the constant-voltage step, the current density also continues to the decrease, which suggests that the insoluble SEI component is more electronically insulating than the soluble species. Interestingly, our EQCM results show that the SEI becomes less soluble as the salt concentration increases. The SEI percentage mass loss decreases from ∼60% for 0.5 M to ∼7% for 4 M, demonstrating that SEI solubility is strongly affected by salt concentration in the electrolyte.

SEI Dissolution and Passivation. Passivity is a key SEI property that directly affects the formation and growth of the interphase, as less passivating layer requires more capacity to inhibit electrolyte reduction. Therefore, the capacity used to form SEI is a good metric for evaluating its passivity. Our EQCM results show that the passivity of the SEI decreases as the salt concentration of the electrolyte is lowered (Figure 2a). When comparing the SEI formation capacity and solubility of different electrolytes (Figure 2b), a positive correlation is obtained regardless of the electrolyte composition, signifying

https://doi.org/10.1021/jacs.3c03195
J. Am. Chem. Soc. XXXX, XXX, XXX−XXX

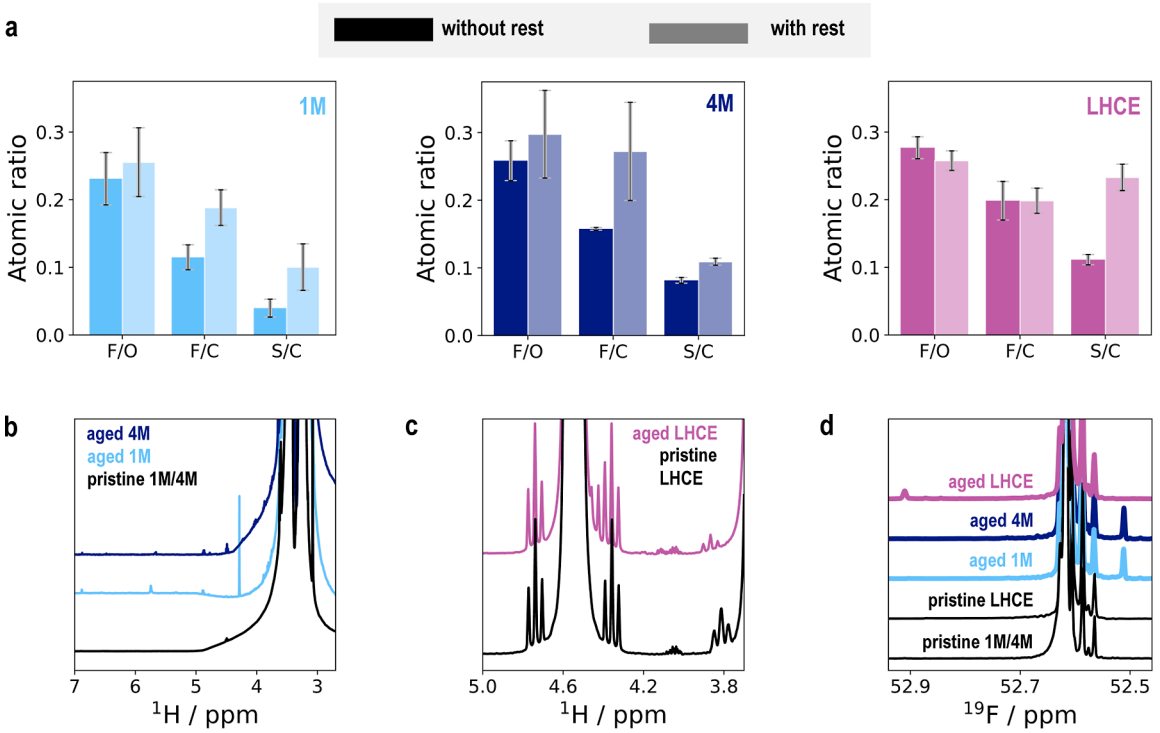

Figure 3. (a) XPS atomic ratios of the SEI grown on copper before and after aging for commonly investigated electrolyte systems such as 1 and 4 M LiFSI in DME (denoted as 1 and 4 M, respectively), and LHCE. Three different spots were sampled during XPS measurements. Electrolytes were aged by soaking it with lithium metal chips for two days. ^{1}H NMR comparison between aged and unaged electrolytes (b) for 4 and 1 M whereas (c) is for LHCE. (d) ^{19}F NMR of aged and unaged electrolytes, where the chemical shift range is near LiFSI peak.

that the two properties are interlinked (Figure 2c). In fact, studies have indicated that more passivating SEIs contain more inorganic species such as LiF and Li_2O.[9,10] However, it is difficult to establish a correlation between SEI solubility and passivity without a systematic quantification of the two properties. Our EQCM results provide additional evidence, suggesting that SEI dissolution is a major mechanism that governs the SEI formation and growth.

Compositional Analysis of SEI and Its Soluble Species. Trends obtained from our EQCM results reveal important fundamental insights involved in the process of SEI dissolution. The negative correlation between electrolyte salt concentration and SEI dissolution (Figure 2b) suggests that an increase in salt concentration could result in less available uncoordinated DME molecules to dissolve SEI components, as well as fewer DME available for the formation of SEI. This is because more DME would be required to fully dissolve LiFSI in the electrolyte. Higher LiFSI concentration can also suppress the dissolution of decomposed Li compounds in the SEI due to the common ion effect. Additionally, our EQCM results show that adding TTE to the LiFSI-DME electrolyte system can suppress SEI dissolution (1.73 M for LHCE compared to 2 M, Figure 2b). Since TTE is a major solvent in LHCE (1.2DME/3TTE molar ratio), the interaction between the SEI and electrolyte in LHCE is expected to be different due to the significant differences between DME and TTE molecules. However, EQCM results alone could not account for the effects of SEI composition on solubility. This is because increasing electrolyte salt concentration or incorporating a diluent into the electrolyte system can result in a more anion-rich Li solvation structure, causing the SEI to be more anion-derived and less soluble.[23−25]

Building upon the insights gained from our EQCM results, we investigate the effect of SEI composition on its solubility by analyzing the interphase's composition before and after dissolution using XPS. To ensure that our results are reliable, three different spots of the SEI formed on copper are analyzed and averaged for all samples investigated. Chemical analysis of the SEI before dissolution shows that 4 M and LHCE form more anion-derived interphases compared to 1 M, agreeing with previous the results published (Figure S3).[23,24] However, LHCE is more anion-derived compared to 4 M, despite its more soluble SEI measured using EQCM (Figure 2b). This illustrates that while anion-derived SEIs are generally less soluble, electrolyte properties such as salt concentration and solvent chemistry can significantly affect dissolution. Based on our results for the LiFSI-DME electrolyte system, the trend between SEI solubility and salt concentration should also apply for other single salt + single solvent electrolytes. This is because at higher concentration, electrolytes will generally exhibit a stronger common ion effect and less free (uncoordinated) solvent molecules and form more anion-derived SEIs.[24,25] However, further theoretical study of SEI dissolution is needed to quantify the contributions of different effects (*e.g.,* common ion effect, availability of uncoordinated solvent molecules, and SEI composition) impacting SEI solubility.

The fact that more anion-derived SEIs are less prone to dissolution (Figure 3a) indicates that organic components in the SEI are more soluble. Therefore, the resulting SEI after dissolution should become more anion-derived and soluble organic moieties should be detectable in the electrolyte. To confirm our hypothesis, compositional changes in the SEI after dissolution were measured using XPS (Figure 3a), revealing

https://doi.org/10.1021/jacs.3c03195
J. Am. Chem. Soc. XXXX, XXX, XXX−XXX

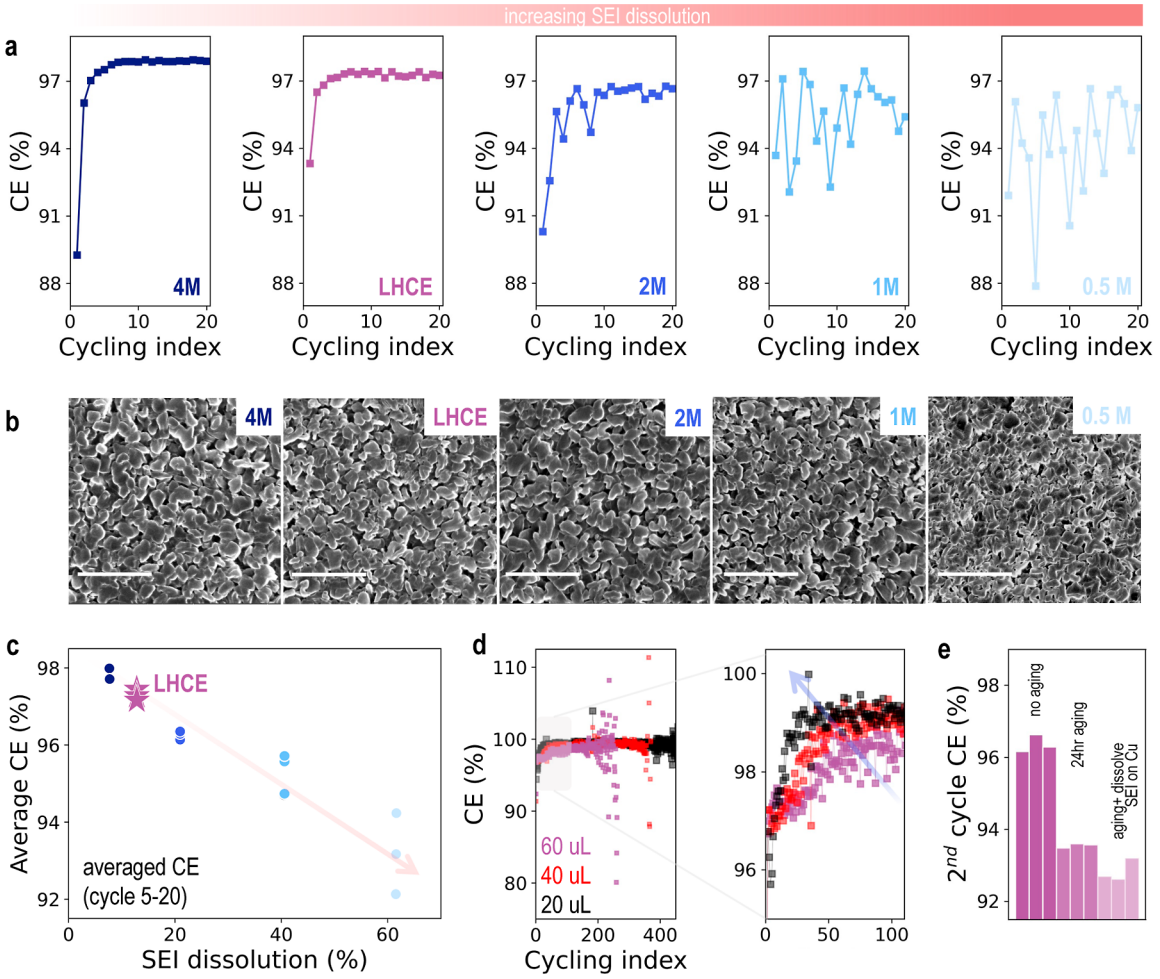

Figure 4. (a) LilCu cycling performance of all electrolytes investigated. 1 mA cm^{-2} current density and 1 mA h cm^{-2} capacity were used during cycling. (b) SEM images of plated Li morphology (first cycle) for the electrolytes investigated. 1 mA cm^{-2} and 1 mA h cm^{-2} were used for the plating conditions. (b) SEM analysis of the first-cycle Li plating morphology for electrolytes investigated. Scale bars, 20 μm. (c) Relationship between average LilCu half-cell cycling CE, averaged between cycles 5−20, and SEI dissolution results from EQCM. (d) LilCu cycling performance using different volumes of LHCE electrolyte. (e) Corrosion study comparing the effect of SEI dissolution (on copper) on corrosion losses. See Figure S5 for detailed cycling protocols. 60 μL of electrolyte is used in all cells unless indicated otherwise.

that all SEIs investigated become more anion-derived after dissolution. Furthermore, the changes in the XPS atomic ratios suggest that the organic soluble species are different for TTE-DME solvent system (LHCE) compared to DME-only electrolytes (1 and 4 M). For 4 and 1 M, the atomic ratios F/O, F/C, and S/C all significantly increased after dissolution, whereas only S/C ratio is increased for LHCE (Figure 3a). This demonstrates that the TTE/DME solvent system interacts differently with the SEI compared to DME only.

Due to its sensitivity, NMR has been widely used to characterize and detect the organic SEI soluble species in carbonate-based electrolytes.[26,27] Herein, we carried out NMR characterization of electrolytes soaked with Li metal chips to detect organic soluble species in the SEI to support our XPS and EQCM results. Soaking Li metal in electrolytes allows the SEI to form chemically on the metal surface, subsequently allowing soluble products to dissolve into the electrolyte media, essentially aging the electrolyte. Comparing NMR spectra of electrolytes with and without aging reveals additional peaks detected primarily in ^{19}F and ^{1}H NMR. Furthermore, different soluble species are detected for the DME-only electrolyte system (1 and 4 M) compared to TTE-DME system (LHCE), corroborating with our XPS analysis. For 1 and 4 M, ^{1}H NMR detects proton peaks around 4−7 ppm, whereas the peaks around 4−4.5 ppm are detected for aged LHCE. This indicates that the soluble species detected (for both DME-only and TTE-DME electrolyte systems) are derived from ether-based molecules (Figure 3b,c).[26] While prior studies report that TTE is not involved in the SEI formation process,[23] our NMR results suggest that it can still interact with solvent-derived components in the SEI. The fact that TTE is fully miscible in DME suggests that the interactions between TTE and solvent-derived SEI components are strong, demonstrating the importance of molecular interactions in SEI solubility.

The positions of 19F NMR peaks for soluble SEI species indicate that there are also soluble species derived from FSI^- anion (Figure 3d). This is because the chemical shifts of these species are close to the fluorine chemical shift in FSI^- anion. We hypothesize that this is a result from reactions between reactive intermediates formed during FSI^- reduction and solvent molecules, yielding organic species that contain sulfonyl fluoride functional groups with similar chemical shift to FSI^- anion.[28] In addition, this would corroborate with the

https://doi.org/10.1021/jacs.3c03195
J. Am. Chem. Soc. XXXX, XXX, XXX−XXX

hydrogen peaks near 7 ppm in ^{1}H NMR, where the protons on the carbon bridging the ether and sulfonyl group would result in a less shielding environment, resulting in higher chemical shift observed.[28] Furthermore, evidence from XPS high-resolution scans underscores the proposed mechanism, where the fluorine peak from $-SO_2F$ decreases in magnitude after the SEI is allowed to dissolve (Figure S4). However, these observations are not present for LHCE. We believe that this is due to the weak interaction between TTE and sulfonyl fluoride functional groups, based on the solubility of LiFSI in TTE compared to LiFSI in DME.[23] Therefore, organic sulfonyl fluoride moieties should be less soluble in LHCE. This is also reflected in our 19F NMR results, where smaller peak near FSI anion is detected for aged LHCE compared to 1 and 4 M. Our findings underscore our hypothesis, suggesting the significance of electrolyte chemistry in SEI dissolution. However, full NMR characterization of SEI soluble species is not possible for our experimental setup, due to the low concentration of the SEI species. Further studies should be done to characterize the structure of SEI soluble species.

Many researchers suggest that anion-derived SEIs are more stable and passivating, which would minimize capacity fading from SEI formation and growth. This is an effective design principle, as more anion-derived SEIs contain more insoluble components.[9−12] However, our results illustrate that it is not only SEI composition that affects its solubility, but also the physical and chemical properties of the electrolyte. More importantly, we show that for high-performance electrolytes (4 M and LHCE), SEI anion composition does not necessarily correlate with the extent of solubility or passivity. As a result, a more quantitative method such as EQCM is needed to evaluate SEI solubility, especially for high-performance electrolytes where electrolyte properties can significantly affect dissolution and anode passivation.

Effects of SEI Dissolution on Li Metal Anode Cyclability. To gauge on how much SEI dissolution affects the cyclability of Li metal anodes, we carried out coulometric experiments to determine whether there is a trend between dissolution and performance. Under regular cycling protocol, our analysis demonstrates a trend where more soluble SEIs result in lower CEs (Figure 4a,c). The average CE (cycle 5−20) ranges from ∼98% for 4 M to ∼93% for 0.5 M. Since the CE is above 95% for the electrolytes investigated (except 0.5 M), capacity loss during cycling should be dominated by SEI formation and growth.[4] This capacity loss pathway depends on two major factors: surface area of electroplated Li metal and SEI passivity. Previous studies and our SEM analyses (Figure 4b) show that the Li plating morphology for these ether-based electrolytes is similar, suggesting that their anode surface areas are comparable.[23,24] Therefore, we believe that it is the passivation problem caused by SEI dissolution that is the dominant mechanism inducing capacity loss for the set of electrolytes investigated here. Dissolution of SEI, which can happen during battery cycling and resting, induces capacity loss from SEI formation and growth. Dissolution causes the SEI to become porous, exposing Li metal to the electrolyte, inducing further electrolyte reduction that forms new SEI layer. The repeated SEI dissolution and reformation do not only result in Li metal inventory loss, but also SEI thickening. In fact, this is a similar mechanism in which SEI dissolution induces capacity fading in graphite-based anodes. However, due to the limited volume expansion of graphite-based anodes during cycling, this problem is not as detrimental in later cycles as the SEI fully passivates the electrode.[5,6] In contrast, LMAs theoretically undergo infinite relative volume change during cycling. This results in new SEIs forming on Li metal surface during every plating step, repeating the cycle of SEI dissolution and maturation.[29] Hence, this partially explains why SEI dissolution could have a more significant effect on cycling performance for LMAs.

A numerical model established by Wood *et al.* predicts that larger electrolyte volume can change SEI solubility equilibria, resulting in accelerated capacity decay and reducing cycle life for Li metal batteries.[7] Building upon their model and our SEI solubility-cyclability trend established, we compare cell cycling utilizing different volumes of LHCE electrolyte. Indeed, our cycling data show that stable cycling is extended to >350 cycles for 20 μL from ∼200 cycles for 60 μL electrolyte volume, with an improvement in CE observed from ∼98.5 to ∼99.2% (averaged over all stable cycles, Figure 4d). Generally, lean electrolyte conditions should result in faster electrolyte consumption, leading to an accelerated capacity decay and cell failure.[30] We believe that this is not the failure mode for the Li|Cu cell configuration used, due to the small capacity (1 mA h cm^{-2}) utilized during battery cycling. Furthermore, the number of cycles it takes for CE to plateau decreases from ∼75 cycles for 60 μL to ∼40 for 20 μL (Figure 4d). We believe that this is due to a faster saturation of SEI soluble species due to less electrolyte volume. This would explain the gradual improvement in CE, as SEI dissolution and growth are minimized when the saturation point is reached. Another factor that could contribute to the faster plateau of CE is the decrease in electroactive surface area when less electrolyte volume is used (less electrolyte wetting). This would result in less galvanic corrosion of Li metal, resulting in an improvement in CE.[8,20] However, the current collector and cell casings do not undergo volume change during cycling, where these surfaces should be passivated within the first five cycles as the SEI mature.[20,31] Therefore, the improved cycling performance observed must be due to the faster saturation of SEI soluble species when lower electrolyte volume is utilized, resulting in less overall SEI dissolution during extended cell cycling.

To further validate our hypothesis suggesting the involvement of SEI dissolution in its formation and growth mechanism, we investigate capacity loss during calendar aging for LHCE by introducing a 24-h resting step at open circuit into the cycling protocol. The rest step is introduced during the second cycle at fully charged state to ensure that the electroactive surface, aside from Li metal surface, is passivated to minimize galvanic corrosion (Figure S5, same protocol used in Boyle *et al.*).[8] Our results show that 24-h calendar aging step induces ∼3% capacity loss (Figure 4e), comparable to other high-performance electrolytes reported previously.[8] However, SEI dissolution can also affect the passivation of other electroactive surface such as the current collector and cell casings. We explored this effect by introducing an additional 24-h resting step at open circuit at the end of the first cycle at fully discharged state, after the 24-h rest in the fully charged state (see Figure S5 for protocol). This allows the SEI on copper and cell casings to dissolve without the interference of corrosion through SEI growth on Li metal surface. Our results show that the overall corrosion loss is only slightly greater when the SEI on copper is allowed to dissolve, suggesting that the additional capacity loss from galvanic corrosion is minimal (Figure 4e). Therefore, we believe that dissolution of the SEI

https://doi.org/10.1021/jacs.3c03195
J. Am. Chem. Soc. XXXX, XXX, XXX−XXX

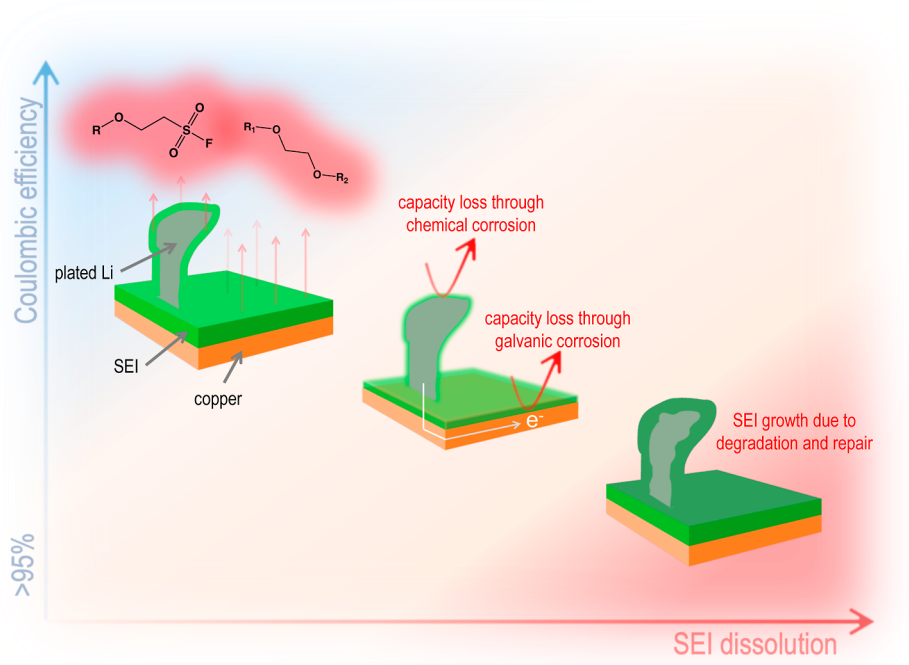

Figure 5. Schematics summarizing SEI dissolution and how it can affect the cycling performance of Li metal anodes.

on Li metal surface is the main contributor toward capacity loss.

Overall, our results suggest that strategies designed to prevent SEI dissolution could push the CE of Li metal anodes higher. Through molecular tuning of the solvent,[32,33] liquid electrolytes can be engineered to purposely decrease its interaction with the SEI to suppress dissolution. By incorporating this into the electrolyte design principle, guided by SEI solubility quantification using EQCM, we believe that both the cycle and calendar life of LMBs can be extended even more effectively through electrolyte engineering.

CONCLUSIONS

Using EQCM, we systematically quantify and compare SEI mass loss from dissolution using electrolytes optimized for LMAs, illustrating that SEIs derived from even state-of-the-art electrolytes undergo significant dissolution during resting at open circuit. The correlation established between solubility and passivity obtained from our EQCM results indicates that SEI dissolution is a major contributor toward SEI formation and growth. Furthermore, we compare our SEI solubility results from EQCM experiments and cycling data to show that the cycle and calendar life of LMAs closely depend on SEI dissolution for high-performance electrolytes (Figure 5). Our results suggest that the cycle life of a state-of-the-art electrolyte can be extended by decreasing SEI dissolution, illustrating that SEI solubility is another knob that can be tuned to effectively minimize the losses from SEI growth. Combining our EQCM results with compositional analyses of the SEI and electrolyte, we show that comparing SEI solubilities solely based its composition becomes less reliable for high-performance electrolytes. Our analyses show that the differences in the amount of anion-derived component in their SEIs become small enough that the physical and chemical properties of the electrolytes start to play a more significant role in dissolution. This provides a crucial piece of information that could help future design of more passivating SEIs through not only tuning the SEI composition, but also tuning the physical and chemical properties of the electrolyte to minimize SEI dissolution even more effectively.

METHODS

Electrolyte Preparation. All electrolytes were prepared and handled in an argon-filled glovebox with an O_2 concentration of <0.2 ppm and H_2O concentration of <0.01 ppm. LiFSI-DME electrolyte was prepared with LiFSI (Oakwood) and DME (Aldrich). LHCE was prepared by adding TTE (SynQuest) to LiFSI in DME solution in a LiFSI/1.2DME/3TTE molar ratio.

EQCM. EQCM measurements were performed using a QCM200 instrument (Stanford Research Systems), where all the electrochemical testing was done in a glovebox filled with argon with an O_2 concentration of <0.2 ppm and H_2O concentration of <0.01 ppm. Testing was done within the sensor holder itself, with a Li metal foil counter electrode. AT-cut quartz crystal coated with copper (Phillip Technologies) was used as the sensor and electrode for electrodeposition.

Electrochemical Methods. Aside from EQCM measurements, electrochemical measurements used 2032-type coin cell with 60 μL of electrolyte (unless specified otherwise). High-quality Li metal foil was used [750 μm, 99.9% (Alfa Aesar)] and Cu foil (Pred Materials) was used for all LilCu cell configuration. Both the Li metal and Cu foil were punched to 1 cm^{-2}. Cu foil was rinsed with deionized water, isopropyl alcohol (Fisher), and acetone (Fisher) before transferring into the glovebox. All 2023-type coin cell assembly used 25-micrometer-thick propylene-polyethylene-propylene (Celgard) as separators. Lithium iron phosphate (2 mA h^{-2}, Targray) was paired with Cu foil for XPS characterization of the SEI before and after dissolution. The SEI was formed on Cu using a constant current−constant-voltage procedure. The current was applied at 50 uA cm^{-2} until the voltage reached 50 mV *vs* Li/Li^+. The voltage was held at this voltage until the current drops down to 10 uA cm^{-2}. For the SEI dissolution experiments, the cells were rested at open circuit for 48 h before cell dissembling and characterization. All battery cycling was carried out at 1 mA cm^{-2} and 1 mA h cm^{-2}. Arbin battery cycler was used to cycle all the cells at 25 °C unless stated otherwise.

https://doi.org/10.1021/jacs.3c03195
J. Am. Chem. Soc. XXXX, XXX, XXX−XXX

XPS. Cu foil working electrodes were prepared in an Ar glovebox, rinsed with 90 μL of DME to remove residual the Li salts, and then transferred to an XPS chamber using a vacuum transfer vessel. XPS signals were collected on a PHI VersaProbe 1 scanning XPS microprobe with an Al Kα source.

NMR. Small pieces of Li metal foil (roughly 1 × 1 × 1 mm size cubes) were soaked in 2 mL of electrolyte for two days. The electrolyte was then filtered through a 0.45-μm polytetrafluoroethylene (PTFE) filter. NMR measurements were performed on a Varian Mercury 400 MHz NMR. The temperature was set at 25 °C. Samples were prepared in the glovebox by injecting 300 μL of electrolyte into a new and dried NMR tube, together with 600 μL of newly opened methyl sulfoxide-d_6 (Acros Organics, 99.9% D, max. 0.03% water impurity in each DMSO-d_6 ampoules). It was then sealed with the PTFE caps and immediately put into the NMR machine for data acquisition. The samples were locked and shimmed using the external standard.

SEM. SEM characterization was carried out in the plated state using Li|Cu cell configuration after 10 cycles. 1 mA cm^{-2} and 1 mA h cm^{-2} was used for the cycling conditions. Characterization was done using Thermo Fisher Scientific Apreo S LoVac Scanning Electron Microscope (SEM).

■ ASSOCIATED CONTENT

Supporting Information

The Supporting Information is available free of charge at https://pubs.acs.org/doi/10.1021/jacs.3c03195.

EQCM profiles, XPS atomic ratio analyses, XPS high-resolution scans, and voltage profiles for calendar aging protocols (PDF)

■ AUTHOR INFORMATION

Corresponding Author

Yi Cui − *Department of Materials Science and Engineering, Stanford University, Stanford, California 94305-6104, United States; Stanford Institute for Materials Energy and Energy Sciences, SLAC National Laboratory, Menlo Park, California 94025, United States;* orcid.org/0000-0002-6103-6352; Email: yicui@stanford.edu

Authors

Philaphon Sayavong − *Department of Chemistry, Stanford University, Stanford, California 94305-6104, United States;* orcid.org/0000-0001-7605-8194

Wenbo Zhang − *Department of Materials Science and Engineering, Stanford University, Stanford, California 94305-6104, United States;* orcid.org/0000-0002-0828-594X

Solomon T. Oyakhire − *Department of Chemical Engineering, Stanford University, Stanford, California 94305-6104, United States;* orcid.org/0000-0002-3189-5949

David T. Boyle − *Department of Chemistry, Stanford University, Stanford, California 94305-6104, United States;* orcid.org/0000-0002-0452-275X

Yuelang Chen − *Department of Chemistry, Stanford University, Stanford, California 94305-6104, United States;* orcid.org/0000-0002-5249-0596

Sang Cheol Kim − *Department of Materials Science and Engineering, Stanford University, Stanford, California 94305-6104, United States;* orcid.org/0000-0002-1749-8277

Rafael A. Vilá − *Department of Materials Science and Engineering, Stanford University, Stanford, California 94305-6104, United States*

Sarah E. Holmes − *Department of Chemistry, Stanford University, Stanford, California 94305-6104, United States;* orcid.org/0000-0002-7946-964X

Mun Sek Kim − *Department of Chemical Engineering, Stanford University, Stanford, California 94305-6104, United States*

Stacey F. Bent − *Department of Chemical Engineering, Stanford University, Stanford, California 94305-6104, United States;* orcid.org/0000-0002-1084-5336

Zhenan Bao − *Department of Chemical Engineering, Stanford University, Stanford, California 94305-6104, United States;* orcid.org/0000-0002-0972-1715

Complete contact information is available at: https://pubs.acs.org/10.1021/jacs.3c03195

Author Contributions

P.S. and W.Z. contributed equally. P.S. and Y.C. conceived the idea. P.S. designed the research with Y.C. guidance. P.S. and D.T.B. conducted the EQCM experiments. P.S. and W.Z. performed the electrochemical testing. S.T.O. conducted the XPS characterization. P.S. and Y.C. conducted the NMR characterization. P.S. and W.Z. carried out the SEM characterization. W.Z., D.T.B., S.C.K., R.A.V., S.E.H., and M.S.K. assisted in results interpretation. P.S., W.Z., and Y.C. wrote the manuscript. All the authors made comments on the manuscript.

Notes

The authors declare no competing financial interest.
All data in the main text or the Supporting Information.

■ ACKNOWLEDGMENTS

We acknowledge support from the Assistant Secretary for Energy Efficiency and Renewable Energy, Office of Vehicle Technologies of the US Department of Energy under the Battery Materials Research (BMR) Program and Battery 500 Consortium. D.T.B. acknowledges support from the National Science Foundation Graduate Research Fellowship Program. S.T.O. acknowledges support from the Knight Hennessy scholarship for graduate studies at Stanford University. R.A.V. acknowledges support from the National Academy of Sciences Ford Foundation Fellowship, the National Science Foundation Graduate Research Fellowship Program (NSF GRFP, grant no. DGE-1656518), and the Enhancing Diversity in Graduate Education (EDGE) Doctoral Fellowship Program at Stanford University. Scanning electron microscopy was performed at the Stanford Nano Shared Facilities (SNSF), supported by the National Science Foundation under award ECCS-1542152. We also acknowledge Christopher E. D. Chidsey for loaning us the SRS QCM200 equipment.

■ REFERENCES

(1) Xu, W.; Wang, J.; Ding, F.; Chen, X.; Nasybulin, E.; Zhang, Y.; Zhang, J.-G. Lithium Metal Anodes for Rechargeable Batteries. *Energy Environ. Sci.* **2014**, *7*, 513−537.

(2) Lin, D.; Liu, Y.; Cui, Y. Reviving the Lithium Metal Anode for High-Energy Batteries. *Nat. Nanotechnol.* **2017**, *12*, 194−206.

(3) Fang, C.; Wang, X.; Meng, Y. S. Key Issues Hindering a Practical Lithium-Metal Anode. *Trends Chem.* **2019**, *1*, 152−158.

(4) Fang, C.; Li, J.; Zhang, M.; Zhang, Y.; Yang, F.; Lee, J. Z.; Lee, M.-H.; Alvarado, J.; Schroeder, M. A.; Yang, Y.; Lu, B.; Williams, N.; Ceja, M.; Yang, L.; Cai, M.; Gu, J.; Xu, K.; Wang, X.; Meng, Y. S. Quantifying Inactive Lithium in Lithium Metal Batteries. *Nature* **2019**, *572*, 511−515.

(5) Broussely, M.; Biensan, Ph.; Bonhomme, F.; Blanchard, Ph.; Herreyre, S.; Nechev, K.; Staniewicz, R. J. Main Aging Mechanisms in Li Ion Batteries. *J. Power Sources* **2005**, *146*, 90−96.

(6) Heiskanen, S. K.; Kim, J.; Lucht, B. L. Generation and Evolution of the Solid Electrolyte Interphase of Lithium-Ion Batteries. *Joule* **2019**, *3*, 2322−2333.
(7) Wood, S. M.; Fang, C.; Dufek, E. J.; Nagpure, S. C.; Sazhin, S. V.; Liaw, B.; Meng, Y. S. Predicting Calendar Aging in Lithium Metal Secondary Batteries: The Impacts of Solid Electrolyte Interphase Composition and Stability. *Adv. Energy Mater.* **2018**, *8*, 1801427.
(8) Boyle, D. T.; Huang, W.; Wang, H.; Li, Y.; Chen, H.; Yu, Z.; Zhang, W.; Bao, Z.; Cui, Y. Corrosion of Lithium Metal Anodes during Calendar Ageing and Its Microscopic Origins. *Nat. Energy* **2021**, *6*, 487−494.
(9) Peled, E.; Menkin, S. Review—SEI: Past, Present and Future. *J. Electrochem. Soc.* **2017**, *164*, A1703−A1719.
(10) Mogensen, R.; Brandell, D.; Younesi, R. Solubility of the Solid Electrolyte Interphase (SEI) in Sodium Ion Batteries. *ACS Energy Lett.* **2016**, *1*, 1173−1178.
(11) Tasaki, K.; Harris, S. J. Computational Study on the Solubility of Lithium Salts Formed on Lithium Ion Battery Negative Electrode in Organic Solvents. *J. Phys. Chem. C* **2010**, *114*, 8076−8083.
(12) Tasaki, K.; Goldberg, A.; Lian, J.-J.; Walker, M.; Timmons, A.; Harris, S. J. Solubility of Lithium Salts Formed on the Lithium-Ion Battery Negative Electrode Surface in Organic Solvents. *J. Electrochem. Soc.* **2009**, *156*, A1019.
(13) Huang, W.; Wang, H.; Boyle, D. T.; Li, Y.; Cui, Y. Resolving Nanoscopic and Mesoscopic Heterogeneity of Fluorinated Species in Battery Solid-Electrolyte Interphases by Cryogenic Electron Microscopy. *ACS Energy Lett.* **2020**, *5*, 1128−1135.
(14) Shadike, Z.; Lee, H.; Borodin, O.; Cao, X.; Fan, X.; Wang, X.; Lin, R.; Bak, S.-M.; Ghose, S.; Xu, K.; Wang, C.; Liu, J.; Xiao, J.; Yang, X.-Q.; Hu, E. Identification of LiH and Nanocrystalline LiF in the Solid−Electrolyte Interphase of Lithium Metal Anodes. *Nat. Nanotechnol.* **2021**, *16*, 549−554.
(15) Kwon, B.; Lee, J.; Kim, H.; Kim, D.; Park, K.; Jo, S.; Lee, K. T. Janus Behaviour of LiFSI- and LiPF6-Based Electrolytes for Li Metal Batteries: Chemical Corrosion versus Galvanic Corrosion. *J. Mater. Chem. A* **2021**, *9*, 24993−25003.
(16) Wang, H.; Matsui, M.; Kuwata, H.; Sonoki, H.; Matsuda, Y.; Shang, X.; Takeda, Y.; Yamamoto, O.; Imanishi, N. A Reversible Dendrite-Free High-Areal-Capacity Lithium Metal Electrode. *Nat. Commun.* **2017**, *8*, 15106.
(17) Sonoki, H.; Matsui, M.; Imanishi, N. Effect of Anion Species in Early Stage of SEI Formation Process. *J. Electrochem. Soc.* **2019**, *166*, A3593−A3598.
(18) Kitz, P. G.; Lacey, M. J.; Novák, P.; Berg, E. J. Operando Investigation of the Solid Electrolyte Interphase Mechanical and Transport Properties Formed from Vinylene Carbonate and Fluoroethylene Carbonate. *J. Power Sources* **2020**, *477*, 228567.
(19) Mozhzhukhina, N.; Flores, E.; Lundström, R.; Nyström, V.; Kitz, P. G.; Edström, K.; Berg, E. J. Direct Operando Observation of Double Layer Charging and Early Solid Electrolyte Interphase Formation in Li-Ion Battery Electrolytes. *J. Phys. Chem. Lett.* **2020**, *11*, 4119−4123.
(20) Lin, D.; Liu, Y.; Li, Y.; Li, Y.; Pei, A.; Xie, J.; Huang, W.; Cui, Y. Fast Galvanic Lithium Corrosion Involving a Kirkendall-Type Mechanism. *Nat. Chem.* **2019**, *11*, 382−389.
(21) Hobold, G. M.; Khurram, A.; Gallant, B. M. Operando Gas Monitoring of Solid Electrolyte Interphase Reactions on Lithium. *Chem. Mater.* **2020**, *32*, 2341−2352.
(22) Yoon, T.; Milien, M. S.; Parimalam, B. S.; Lucht, B. L. Thermal Decomposition of the Solid Electrolyte Interphase (SEI) on Silicon Electrodes for Lithium Ion Batteries. *Chem. Mater.* **2017**, *29*, 3237−3245.
(23) Ren, X.; Zou, L.; Cao, X.; Engelhard, M. H.; Liu, W.; Burton, S. D.; Lee, H.; Niu, C.; Matthews, B. E.; Zhu, Z.; Wang, C.; Arey, B. W.; Xiao, J.; Liu, J.; Zhang, J.-G.; Xu, W. Enabling High-Voltage Lithium-Metal Batteries under Practical Conditions. *Joule* **2019**, *3*, 1662−1676.
(24) Qian, J.; Henderson, W. A.; Xu, W.; Bhattacharya, P.; Engelhard, M.; Borodin, O.; Zhang, J.-G. High Rate and Stable Cycling of Lithium Metal Anode. *Nat. Commun.* **2015**, *6*, 6362.
(25) Kim, S. C.; Kong, X.; Vilá, R. A.; Huang, W.; Chen, Y.; Boyle, D. T.; Yu, Z.; Wang, H.; Bao, Z.; Qin, J.; Cui, Y. Potentiometric Measurement to Probe Solvation Energy and Its Correlation to Lithium Battery Cyclability. *J. Am. Chem. Soc.* **2021**, *143*, 10301−10308.
(26) Jin, Y.; Kneusels, N.-J. H.; Grey, C. P. NMR Study of the Degradation Products of Ethylene Carbonate in Silicon−Lithium Ion Batteries. *J. Phys. Chem. Lett.* **2019**, *10*, 6345−6350.
(27) Wang, L.; Menakath, A.; Han, F.; Wang, Y.; Zavalij, P. Y.; Gaskell, K. J.; Borodin, O.; Iuga, D.; Brown, S. P.; Wang, C.; Xu, K.; Eichhorn, B. W. Identifying the Components of the Solid−Electrolyte Interphase in Li-Ion Batteries. *Nat. Chem.* **2019**, *11*, 789−796.
(28) Xu, R.; Xu, T.; Yang, M.; Cao, T.; Liao, S. A Rapid Access to Aliphatic Sulfonyl Fluorides. *Nat. Commun.* **2019**, *10*, 3752.
(29) Li, Y.; Huang, W.; Li, Y.; Pei, A.; Boyle, D. T.; Cui, Y. Correlating Structure and Function of Battery Interphases at Atomic Resolution Using Cryoelectron Microscopy. *Joule* **2018**, *2*, 2167−2177.
(30) Nagpure, S. C.; Tanim, T. R.; Dufek, E. J.; Viswanathan, V. V.; Crawford, A. J.; Wood, S. M.; Xiao, J.; Dickerson, C. C.; Liaw, B. Impacts of Lean Electrolyte on Cycle Life for Rechargeable Li Metal Batteries. *J. Power Sources* **2018**, *407*, 53−62.
(31) Kolesnikov, A.; Kolek, M.; Dohmann, J. F.; Horsthemke, F.; Börner, M.; Bieker, P.; Winter, M.; Stan, M. Galvanic Corrosion of Lithium-Powder-Based Electrodes. *Adv. Energy Mater.* **2020**, *10*, 2000017.
(32) Yu, Z.; Wang, H.; Kong, X.; Huang, W.; Tsao, Y.; Mackanic, D. G.; Wang, K.; Wang, X.; Huang, W.; Choudhury, S.; Zheng, Y.; Amanchukwu, C. V.; Hung, S. T.; Ma, Y.; Lomeli, E. G.; Qin, J.; Cui, Y.; Bao, Z. Molecular Design for Electrolyte Solvents Enabling Energy-Dense and Long-Cycling Lithium Metal Batteries. *Nat. Energy* **2020**, *5*, 526−533.
(33) Yu, Z.; Rudnicki, P. E.; Zhang, Z.; Huang, Z.; Celik, H.; Oyakhire, S. T.; Chen, Y.; Kong, X.; Kim, S. C.; Xiao, X.; Wang, H.; Zheng, Y.; Kamat, G. A.; Kim, M. S.; Bent, S. F.; Qin, J.; Cui, Y.; Bao, Z. Rational Solvent Molecule Tuning for High-Performance Lithium Metal Battery Electrolytes. *Nat. Energy* **2022**, *7*, 94−106.

https://doi.org/10.1021/jacs.3c03195
J. Am. Chem. Soc. XXXX, XXX, XXX−XXX